RSC Advances

PAPER

View Article Online
View Journal | View Issue

Cite this: *RSC Adv.*, 2022, **12**, 27253

Synergistic effects of CNTs/SiO_2 composite fillers on mechanical properties of cement composites

Shaojie Li,[a] Ping Shen,[b] Hang Zhou,[a] Shiguo Du,[a] Yuling Zhang *[a] and Jun Yan*[c]

This paper investigated the hybridization use of carbon nanotubes (CNTs) with nano-SiO_2 in cement composites. The (CNTs)/SiO_2 composite fillers were designed and prepared by electrostatic self-assembly technology to reinforce cement composites. The mechanical properties, microstructure and hydration characteristics of cement composites incorporating CNTs/SiO_2 fillers were systematically researched. The morphology and optical microscopy results show that the CNTs inside CNTs/SiO_2 fillers tended to unwind due to the mechanical separation and steric hindrance of nano-SiO_2 particles with certain size, and its agglomeration degree in the suspension greatly alleviated over time. With the appropriate incorporation of CNTs/SiO_2 fillers (containing 0.10 wt% CNTs and 0.50 wt% nano-SiO_2), the flexural strength, compressive strength and flexural toughness of the cement mortar matrix were sharply increased by 33.5%, 36.5% and 56.0% after curing for 28 days compared to the plain sample, respectively. Microscopic observations show that appropriate nano-additives can densify and refine the hydrated microstructure, and the crack-bridging, debonding and pull-out behaviors of CNTs were all observed. Hydration analysis quantitatively reveals that CNTs/SiO_2 fillers significantly accelerated the cement hydration process by virtue of the nano-nucleating action. The reinforcing mechanisms of CNTs/SiO_2 fillers can be attributed to the proposed synergistic effects of CNTs/SiO_2 fillers, which mainly include the better dispersion stability of CNTs, the nucleating effect of nano-additives and the pozzolanic reaction by nano-SiO_2, thus positively leading to increased mechanical properties.

Received 4th July 2022
Accepted 19th September 2022

DOI: 10.1039/d2ra04127h

rsc.li/rsc-advances

1. Introduction

Cement-based composites represented by concrete have long occupied quite important positions in military protective engineering due to their low cost and superior performance, and will continue to play an increasingly important role in the future. However, some inherent severe drawbacks of cement-based materials, such as remarkable brittleness, low tensile strength and proneness to crack, largely affect the safety, applicability and durability of the overall structure, which struggle to meet the growing demands of protective engineering construction. To develop high-performance or multifunctional cementitious materials, many attempts have been carried out to incorporate a wide range of reinforcements into the matrix, such as steel fibers,[1–4] carbon fibers,[5–8] polymer fibers[9,10] *etc.* However, it has been proven that these traditional fibers are more effective at the macro scale than the micro scale, which fail to refine internal microstructure and positively regulate the hydration process.[11,12] Therefore, given the fact that nano-sized hydrated calcium silicate (C–S–H) gels are the main cement hydration phases, it is more effective to improve the microstructure of cement-based materials at the nanoscale.

The recent development in nanotechnology renders nanomaterials attractive for their applications in improving the performance of cement composites. Some representative nanomaterials, such as carbon nanotubes (CNTs),[13–17] nano-SiO_2,[18–20] nano-TiO_2,[21,22] nano-Al_2O_3,[23,24] and so on, have brought invaluable possibility to the reinforcement of cement matrix. Among them, the CNTs, featuring ultra-high tensile strength and elastic modulus, are considered as the promising and competitive candidates for the use as nano-reinforcers in cement composites. It is expected that CNTs can significantly refine the microstructure of matrix as the result of nano-filling and nucleating effects during cement hydration. Especially, according to previous studies, CNTs can also exhibit the superior abilities of bridging cracks and mitigating cracks propagation at the nanoscale due to the unique tube-shaped structure with large aspect ratio.[25–28]

Currently, achieving the efficient dispersion of CNTs and favorable interfacial bonding strength between CNTs and cement matrix are the still unremittingly pursuing goals, which is expected to establish effective guidelines for the incorporation of CNTs in the specific matrix environment. Furthermore, more systematic studies deserve to be carried out about the

[a]*Army Engineering University, Shijiazhuang 050003, China. E-mail: zhangyuling2009@163.com*

[b]*Institute of Chemistry, Chinese Academy of Sciences, Beijing 100190, China*

[c]*Hebei Jiaotong Vocational and Technical College, Shijiazhuang 050003, China. E-mail: yan-junjun@263.net*

mechanical properties, durability and reproducibility of CNTs reinforced cement composites. The hydrophobicity, high aspect ratio, coupled with strong van der Waals forces, commonly contribute to the inherent agglomeration bias of CNTs, which may be a reasonable interpretation for that the final reinforcing efficiency of CNTs is much lower than the theoretical value. Although the initial dispersion can be obtained by combining mechanical ultrasonication with chemical surfactants,[29–34] this equilibrium is easily broken with the extended time or varied external environment. Additionally, the surface functional modifications represented by strong oxidation of concentrated acid tend to introduce damage on CNTs surfaces in addition to operation difficulty and environment pollution.[35–38] A highly effective dispersion solution that displays practicable potential has not yet been proposed in term of industrial preparation, which is the imperative step towards designing the desirable composites.

Meanwhile, nano-SiO_2 particles have received increasing interests for their promising applications in cement composites. With the higher specific surface area, it has been reported that nano-SiO_2 particles possess much higher pozzolanic activity with respect to other mineral admixtures.[39] According to previous studies, nano-SiO_2 can promote C–S–H gels formation and reduce crystalline calcium hydroxide (CH) content, which substantially densify the microstructure and optimize interface transition zone of composites.[20,21,40–43] Therefore, it may be an effective strategy to utilize nano-SiO_2 as spatial barrier to achieve favorable dispersion of CNTs. It is inspiring to innovatively combine CNTs with nano-SiO_2 particles for achieving the desirable synergistic reinforcing effects. Presently, few related researches have been systematically conducted.

In this study, the CNTs/SiO_2 composite fillers were prepared by the simple electrostatic self-assembly method. The morphology and dispersion stability of the prepared composite fillers were researched by electron microscope and optical microscopy. The synergistic reinforcing effects of CNTs/SiO_2 fillers on cement composites were investigated. Based on the systematic analysis including mechanical properties, microstructure and hydration characteristics of cement mortars reinforced by nano-additives, the reinforcing mechanisms of CNTs/SiO_2 fillers were proposed. This work provides an effective strategy for the hybridization use of nanomaterials in cement composites.

2. Experimental methods

2.1 Materials

The multi-walled CNTs were provided by Chengdu Organic Chemicals Co. Ltd, China, and their properties are shown in Table 1. Amorphous nano-SiO_2 particles were purchased from Shanghai Aladdin Biochemical Technology Co. Ltd, China, and were used as received without any further treatment, and their properties are listed in Table 2. Cationic surfactant CTAB ($C_{16}H_{33}(CH_3)_3NBr$, AR), provided by Aladdin, was used to disperse CNTs and regulate positive electricity of CNTs surfaces. Commercially available ordinary Portland cement P.O 52.5R and standard sand (Xiamen Aisio Standard Sand Co. Ltd, China) was used to fabricate cement mortars in this experiment. Polycarboxylate superlasticizer provided by Sobute New Materials Co. Ltd was used to ensure well workability of fresh paste.

Table 1 Properties of CNTs

Diameter	Length	True density	Purity	Specific surface area
10–20 nm	10–30 μm	~2.1 g cm^{-3}	>98%	220–300 m^2 g^{-1}

Table 2 Properties of nano-SiO_2

Mean particle size	True density	Purity	Specific surface area
~15 nm	~2.6 g cm^{-3}	>99.5%	150–200 m^2 g^{-1}

2.2 Preparation of electrostatic self-assembled CNTs/SiO_2 fillers

The electrostatic self-assembled technology paves an effective and simple way for the design of excellent nano-composites. In this study, cationic CTAB was selected as chemical modification agent to regulate electrical properties as well as disperse CNTs. According to other reports, cationic CTAB exhibits the preferable advantage in separating CNTs owing to their preferential attraction toward negatively charged CNTs surfaces.[44,45] In this research, considering the full adsorption of CTAB on CNTs surfaces, the ratio of CTAB to CNTs was identified as 2 : 1 by weight. To prepare CNTs suspensions, 0.40 wt% CTAB were firstly added to 100 mL water followed by even stirring for 2 min to promote full dissolution. Then 0.20 wt% CNTs powder were added to the above solution and stirred until CNTs were completely wetted. The obtained mixture was subjected to ultrasonic vibration for 10 min at 400 W using an ultrasonic disrupter (Scientz-1500F). The positively charged CNTs suspensions were then obtained.

A certain amount of nano-SiO_2 particles were dispersed in 100 mL deionized water by ultrasonic vibration for 5 min at 400 W. To prepare self-assembled CNTs/SiO_2 suspensions, nano-SiO_2 dispersions were mixed with the prepared CNTs suspensions under magnetic stirring for 30 min to facilitate sufficient interactions between positively charged CNTs and nano-SiO_2. Then the composite fillers were prepared after centrifugation, washing with deionized water, and freeze-drying for further characterization analysis. To determine the optimal ratio of nano-SiO_2 to CNTs in CNTs/SiO_2 composite fillers, the

Table 3 Composition of CNTs/SiO_2 fillers[a]

Sample	CNTs (wt%)	SiO_2 (wt%)
C_1Si_1	0.20	0.20
C_1Si_3	0.20	0.60
C_1Si_5	0.20	1.00

[a] The percentages refer to the initial weight fractions of CNTs and SiO_2 in their respective suspensions.

mass ratios of CNTs to nano-SiO_2 in this experiment were set at 1 : 1, 1 : 3 and 1 : 5, respectively. Thus, the prepared fillers were labelled as C_1Si_1, C_1Si_3 and C_1Si_5 accordingly, and the detailed compositions were listed in Table 3.

2.3 Fabrication of cement mortars

The cement mortar specimens were prepared according to the mix proportions shown in Table 4. Four kinds of specimens were prepared in the experiment, *i.e.*, the plain sample (without any nano-additives), the CC sample (with CNTs only), the SC sample (with nano-SiO_2 particles only) and the HC samples (with self-assembled CNTs/SiO_2 fillers). The ratio of water to cement was kept at 0.4, and the sand-to-cement ratio was 3 for all preparations. Water used for the nano-additives suspensions (CNTs, nano-SiO_2 particles, CNTs/SiO_2 fillers, respectively) equaled to the total required water. In addition, considering the influence of nano-additives on fluidity, superplasticizer was added at amount of 0.6% by weight of cement in all specimens.

The mixing process was completed in a standard mixer. Firstly, the suspension of nano-additives was mixed with cement at low speed for 60 s and at high speed for 30 s. Then the superplasticizer and sand were placed into the mixer and stirred for 120 s at high speed. In accordance with Chinese standard GB/T 2419-2005, the mini-slump test was conducted to test fluidity immediately after mixing process. Then the resulting mixture was poured into molds of 40 mm × 40 mm × 160 mm in size, followed by vibration for compaction on a vibration table. Specimens were removed from molds after 24 h and cured under standard conditions until mechanical strength tests.

2.4 Characterization and testing

The prepared series of CNTs/SiO_2 suspensions in Section 2.2 were characterized using transmission electron microscope (TEM, JEOL JEM-2100) operating at 200 kV. The supernatants of suspensions were diluted 10 times and then dropped onto copper grids. The dispersed morphology of composite fillers was observed after drying. The morphology of electrostatic self-assembled CNTs/SiO_2 fillers was also observed by scanning electron microscope (SEM, ZEISS Gemini 300). The functional groups characteristics of nano-additives were measured by Fourier transform infrared spectroscopy (FTIR, Bruker TENSOR II) and X-ray photoelectron spectroscopy (XPS, Thermo EscaLab 250XI). The dispersion state of prepared CNTs/SiO_2 suspensions at different times was evaluated using a typical optical microscope (ToupTek Photonics). The contact angle tests of composite fillers were conducted on a contact angle tester (Dataphysics OCA40). The test was repeated twice for each sample, and the average value was taken as the final result.

Mechanical tests of cement mortar specimens include flexural strength and compressive strength. The flexural strength test was conducted on a universal electronic testing machine (Instron 5982) at constant loading rate of 0.2 mm min^{-1}. The compressive strength test was carried out on a compression testing machine (Sanyu HYE-300B) at a loading rate of 2400 ± 200 N s^{-1}. For morphology and microstructure analysis, appropriate fragments in size were collected from broken specimens after mechanical tests, and were immersed in absolute ethanol for 24 h to hamper further hydration. The fracture surfaces of samples were observed by SEM. Thermogravimetric tests of samples were conducted by a thermal analyzer (TG, NETZSCH TG 209F1) at nitrogen atmosphere with the flow velocity of 100 mL min^{-1}. The temperature range was from room temperature to 1000 °C, and the heating rate was 10 °C min^{-1}. X-ray powder diffraction (XRD, Bruker D8 Advance) was applied to determine the crystalline phase composition in different cement mortar samples. The scanning rate was 0.02° s^{-1} in a 2θ range of 10–70°.

3. Results and discussion

3.1 Characterization of electrostatic self-assembled CNTs/SiO_2 fillers

Prior to the preparation experiment, the microstructure and surface morphology of raw materials were characterized firstly. The FTIR spectra and XRD patterns of raw materials are shown in Fig. 1 and 2, respectively. The characteristic peaks of CNTs at 3441 and 1639 cm^{-1} indicated the H–O–H stretching and bending vibration modes, which can be attributed to the absorbed H_2O molecules. The FTIR spectra of SiO_2 clearly revealed several absorption peaks at 1108, 977, 806 and 475 cm^{-1}, corresponding to Si–O–Si asymmetric stretching vibration, Si–OH bending vibration, Si–O–Si symmetric stretching vibration and Si–O–Si bending vibration, respectively.[43] The peaks appearing at 3446 and 1636 cm^{-1} were allotted to stretching and bending vibration modes of hydrated O–H. In Fig. 2, the distinctive diffractive peaks at 26° and 43° of CNTs were indexed as the (002) and (100) reflections of the hexagonal graphitic structure, and the wide peak between 15° and 30° corresponded to the amorphous structure of nano-SiO_2

Table 4 Mix proportions for cement mortars and fluidity results[a]

Samples	*w/c*	Sand (wt%)	CNTs (wt%)	SiO_2 (wt%)	Superplasticizer (wt%)	Fluidity (mm)
Plain	0.4	300	0	0	0.6	175
CC	0.4	300	0.10	0	0.6	168
SC	0.4	300	0	0.50	0.6	172
HC05	0.4	300	0.05	0.25	0.6	170
HC10	0.4	300	0.10	0.50	0.6	165
HC20	0.4	300	0.20	1.00	0.6	156

[a] The percentages are calculated by weight of cement.

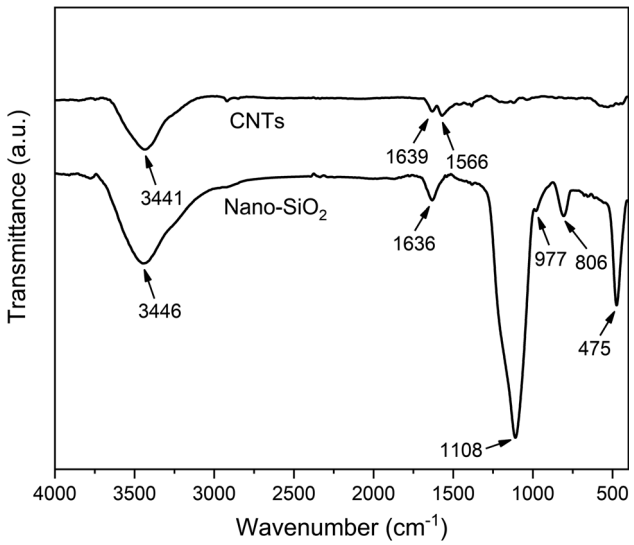

Fig. 1 FTIR spectra of CNTs and nano-SiO_2.

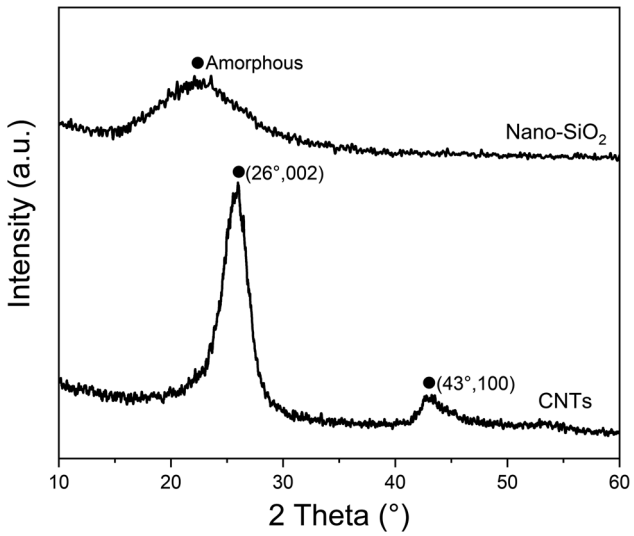

Fig. 2 XRD patterns of CNTs and nano-SiO_2.

particles.[46] Furthermore, the morphology of nano-SiO_2 particles is shown in Fig. 3(a) and (b). It can be found that nano-SiO_2 particles severely tended to agglomerate due to the large specific surface area, given the fact that they were observed using TEM after ultrasonic treatment.

The surface morphologies of CNTs/SiO_2 fillers were observed by SEM, as shown in Fig. 4. It can be seen in Fig. 4(a) that CNTs tended to intertwine with each other and form bundles due to the high surface area and strong van der Waals forces between adjacent tubes. In contrast, CNTs were relatively uniformly separated by varied amounts of nano-SiO_2 particles after electrostatic self-assembled treatment. As the nano-SiO_2 concentration increased, more nano-SiO_2 particles were adsorbed on positively charged CNTs surfaces by electrostatic interaction thus forming CNTs/SiO_2 fillers, which are shown in Fig. 4(b)–(d). It is remarkable that the agglomerating and intertwining

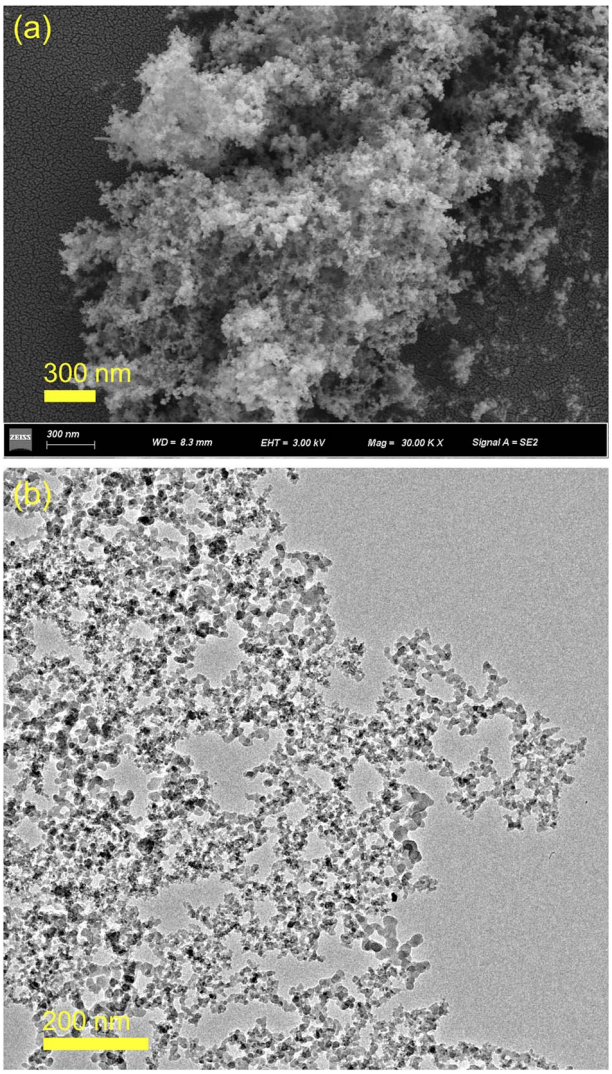

Fig. 3 SEM image (a) and TEM image (b) of nano-SiO_2.

degree of CNTs greatly weakened in composite fillers which is preferably beneficial for their dispersion in matrix. FTIR and XPS analyses were conducted to clarify the surface chemical characteristics of composite fillers. As presented in Fig. 5, the main characteristic absorption peaks containing Si had no obvious location shift while their intensity sharply increased with the increased nano-SiO_2 content. Noticeably, the absorption peak of H–O–H group displayed an obvious red shift from 1651 cm^{-1} to 1635 cm^{-1}, which resulted most likely from the more structural water introduced by nano-SiO_2. The weak absorption peaks at 2926 and 2845 cm^{-1} demonstrated the existence of methylene groups, indicating the effective adsorption of CTAB on CNTs surfaces. The XPS spectra showed consistent results with the FTIR results, which could be seen in Fig. 6. The Si 2p and N 1s characteristic peaks can be clearly found in the survey spectra of CNTs/SiO_2 fillers. The Si and O content significantly increased with the decreased C content following the sequence from C_1Si_1 to C_1Si_5, indicating the higher SiO_2 content in the corresponding sample, and Only C and O can be found in the XPS result of CNTs. Furthermore, the

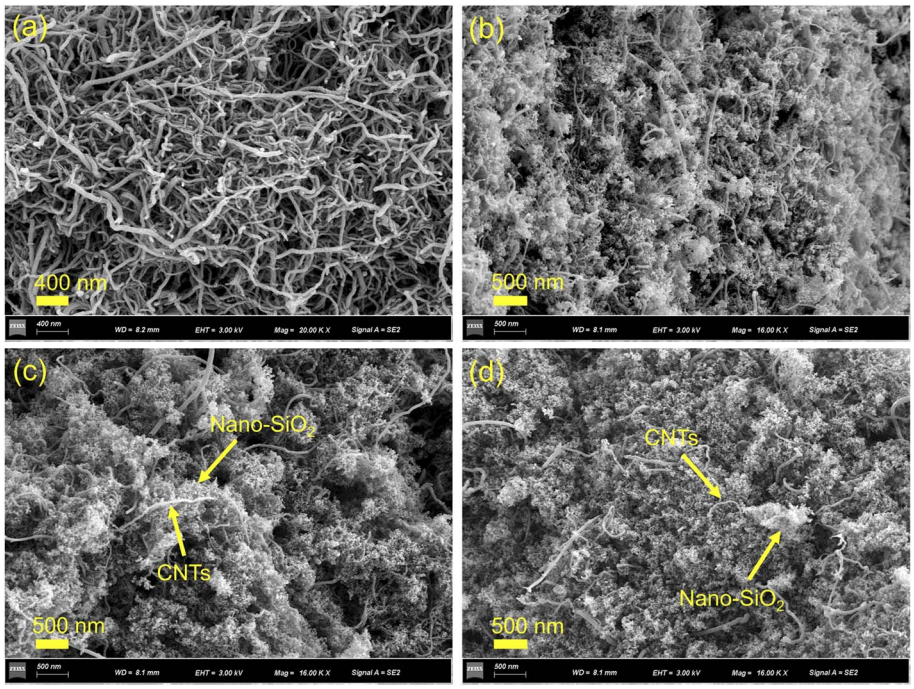

Fig. 4 SEM images of pristine CNTs (a) and electrostatic self-assembled C_1Si_1 (b), C_1Si_3 (c), C_1Si_5 (d).

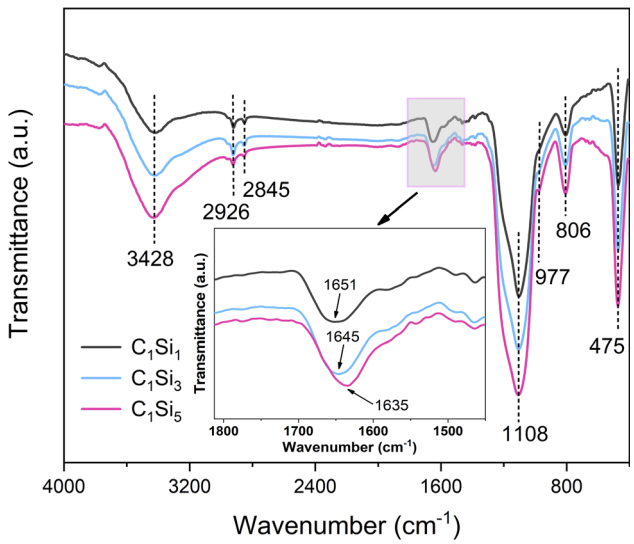

Fig. 5 FTIR spectra of electrostatic self-assembled C_1Si_1, C_1Si_3 and C_1Si_5.

high-resolution C 1s spectra of CNTs and C_1Si_5 were compared at Fig. 6(b). The two peaks appearing at 284.3 eV and 285.2 eV of CNTs can be attributed to the chemical bonds of C–C and C–O, respectively. The C_1Si_5 exhibited the similar C 1s spectra, but the new broad peak with low intensity appeared at 286.1 eV, which can be assigned to C–N bonds, indeed indicating the existence of CTAB. In addition, the high-resolution Si 2p and N 1s spectra of C_1Si_5 were presented in Fig. 6(c) and (d). The characteristic peak at 103.8 eV was all ascribed to Si–O bonds, which singly resulted from the absorbed SiO_2.[47] For the N 1s spectra in Fig. 6(d), the peaks at 399.2 eV and 401.8 eV, corresponding to C–N and Br–N bonds, were considered to be from internal bonds from CTAB. Based on the above results, it's can be verified that there were no new covalent interactions to be detected between CNTs and nano-SiO_2 nanoparticles during the preparation process of CNTs/SiO_2 fillers.

3.2 Dispersion efficiency of CNTs/SiO_2 fillers

To further visualize the morphology and dispersion state of CNTs/SiO_2 fillers with different proportions, the samples from CNTs/SiO_2 suspensions were observed by TEM. As shown in Fig. 7(a), raw CNTs intertwined severely, featuring relatively smooth surface, which is consistent with the results shown by SEM. In contrast, the dispersion of CNTs/SiO_2 fillers was more uniform, and the well-dispersed CNTs were most likely detected as individual tube at the same scale. The CNTs and different content nano-SiO_2 spontaneously assembled into the approximate "grape string" structure, in which CNTs served as the stem and the attached nano-SiO_2 acted as the grapes (Fig. 7(b)). The amount of nano-SiO_2 attached on CNTs surfaces varied with mixing proportion changes. Especially, it can be seen from Fig. 7(e) and (f) that considerable amounts of nano-SiO_2 particles uniformly and densely distributed on CNTs surfaces as the composite fillers C_1Si_5 possessed the highest nano-SiO_2 percentage. In addition, the typical contact angles tests of composite fillers are shown in Fig. 7(g–i). With nano-SiO_2 percentage increasing, the surface hydrophilicity of CNTs/SiO_2 fillers significantly increased due to the abundant presence of hydrophilic Si–OH on SiO_2 surfaces, which is favourable for the stable dispersion in aqueous solution. Given the fact that the fillers C_1Si_5 possess the relatively uniform nano-SiO_2

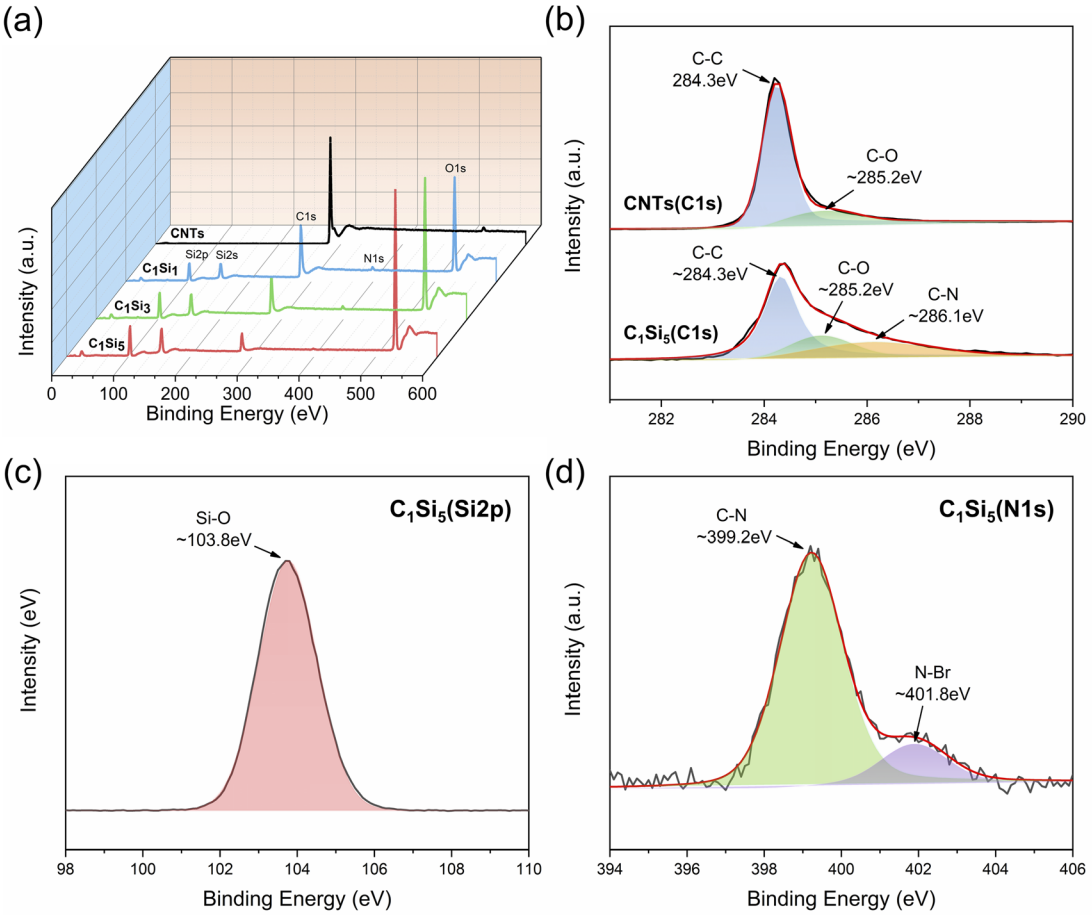

Fig. 6 (a) XPS survey spectra of CNTs and CNTs/SiO_2 fillers; (b) high-resolution C 1s spectra of CNTs and C_1Si_5; (c) high-resolution Si 2p spectra of C_1Si_5; (d) high-resolution N 1s spectra of C_1Si_5.

distribution and excellent hydrophilicity, the assembly ratio of CNTs to nano-SiO_2 particles is adopted as 1 : 5 in the following experiments.

Moreover, to better investigate the dispersion state and stability of the composite fillers, optical microscopy observations for C_1Si_5 and CNTs in aqueous solutions were carried out, and the results are presented in Fig. 8. Both freshly prepared C_1Si_5 and CNTs suspensions exhibited effective dispersion at initial time after appropriate ultrasonication, with a few agglomerates being viewed, as observed in Fig. 8(a) and (c). However, after standing for 24 h, large amounts of slight and small C_1Si_5 agglomerates were observed (Fig. 8(b)), while severe agglomeration behaviour occurred in CNTs suspension (Fig. 8(d)). The composite fillers C_1Si_5 feature strong hydrophilicity, and the CNTs inside fillers are mechanically separated by small nano-SiO_2 agglomerates, thus leading to the excellent dispersion stability of C_1Si_5 suspension. The microscope results show good consistency with the TEM results, indicating the favorable dispersion stability of CNTs can be achieved in the aqueous solution of CNTs/SiO_2 fillers with the optimum assembly ratio.

The CNTs/SiO_2 fillers were prepared using physical blending technology driven by electrostatic interactions, and the mechanism are shown in Fig. 9. As the frequently-used cationic surfactant, CTAB is adsorbed on CNTs surfaces with the long alkyl chains, and endow CNTs with electro-positivity as a result of ionization in aqueous solution.[48] Thus, the CNTs can be dispersed initially by the combined electrostatic–steric hindrance action of CTAB. The surfaces of inorganic nano-SiO_2 particles are usually negatively charged due to the ionization of hydrophilic Si–OH. Therefore, the CNTs/SiO_2 fillers with the "grape string" structure can be obtained by assembling charged CNTs and nano-SiO_2 particles driven by electrostatic attraction. The nano-SiO_2 particles hybridized with CNTs can function as the spatial barrier, and protect the CNTs from interwinding with each other, thus facilitating the stable dispersion of CNTs.

3.3 Fluidity and mechanical properties

The effect of nano-additives on the fluidity of cement mortars was investigated, as shown in Table 4. It can be found that the fluidity decreased with the addition of nanomaterials, and HC20 showed the poorest fluidity of about 156 mm with the decrease of 11% compared to plain sample. The main reason resulting in degradation of fluidity can be attributed to the fact that the nano-additives after ultrasonication increase the

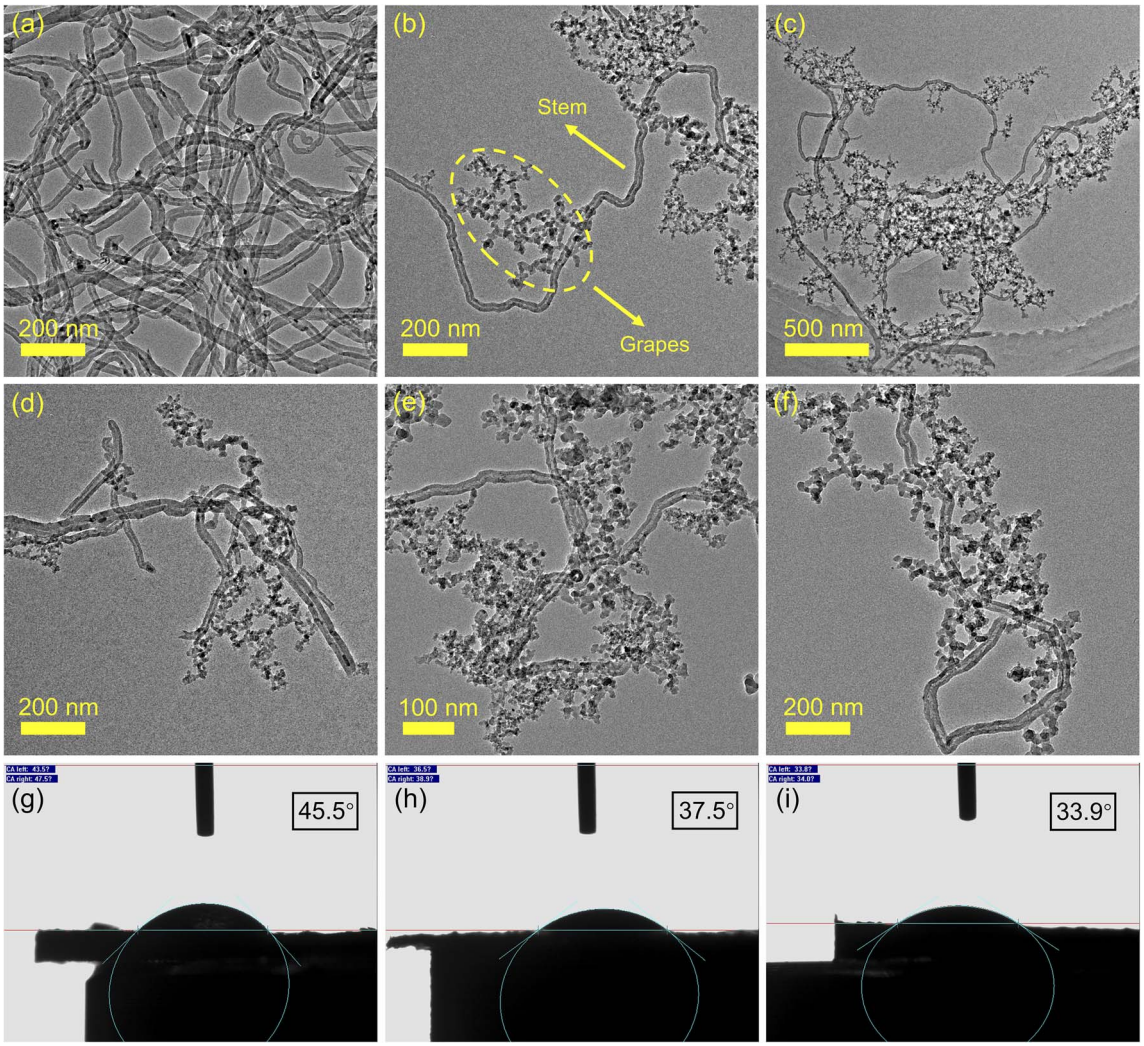

Fig. 7 TEM images of pristine CNTs (a) and electrostatic self-assembled C_1Si_1 (b), C_1Si_3 (c and d), C_1Si_5 (e and f); typical contact angles of C_1Si_1 (g), C_1Si_3 (h) and C_1Si_5 (i).

viscosity of cement mortars. This influence is more remarkable with the continued increase of nanomaterials.

The flexural and compressive strengths of cement mortars containing different nano-reinforcement after curing for 7 and 28 days are presented in Fig. 10. It can be clearly noted that the incorporation of nano-additives all exerted positive influence on mechanical behaviour to some extent, verifying the nano-reinforcing effect of these nanomaterials reported previously. For the CC and SC samples, the mechanical properties were improved slightly compared to plain sample at 7 and 28 days. The underlying reinforcement mechanism can be attributed to the combination of refined microstructure and accelerated hydration. Notably, the CNTs/SiO_2 fillers displayed the similar but stronger reinforcement effects compared to CNTs or nano-SiO_2 alone. The HC10 showed the highest flexural and compressive strengths, which were much higher than those of cement mortars containing single-promoter (CC or SC). Compared to plain sample, the flexural and compressive strengths were sharply increased by 36.8% and 35.3% at 7 days, while the corresponding enhancement rates were 33.5% and 36.5% at 28 days, respectively. These results indicate that the CNTs/SiO_2 fillers exerted favourably synergistic reinforcement effects on mechanical properties, which were more prominent in early cement hydration ages. More details about the mechanism will be discussed in Section 3.6. However, it is worth to note no further increase in mechanical performance occurred for the HC20 sample when more CNTs/SiO_2 fillers were added. The higher fillers concentration may lead to the formation of agglomerates again, which are detrimental to the fluidity and mechanical strengths.

Moreover, the flexural load–displacement curves of samples after 28 days curing are shown in Fig. 11, and the corresponding test results are summarized in Table 5. Flexural toughness refers to the energy absorption until failure, which is calculated based on the total area under the load–displacement curves.[27,49] In this research, flexural toughness was presented as the relative value to that of plain sample. The results indicate that the flexural toughness of cement mortar all increased with the

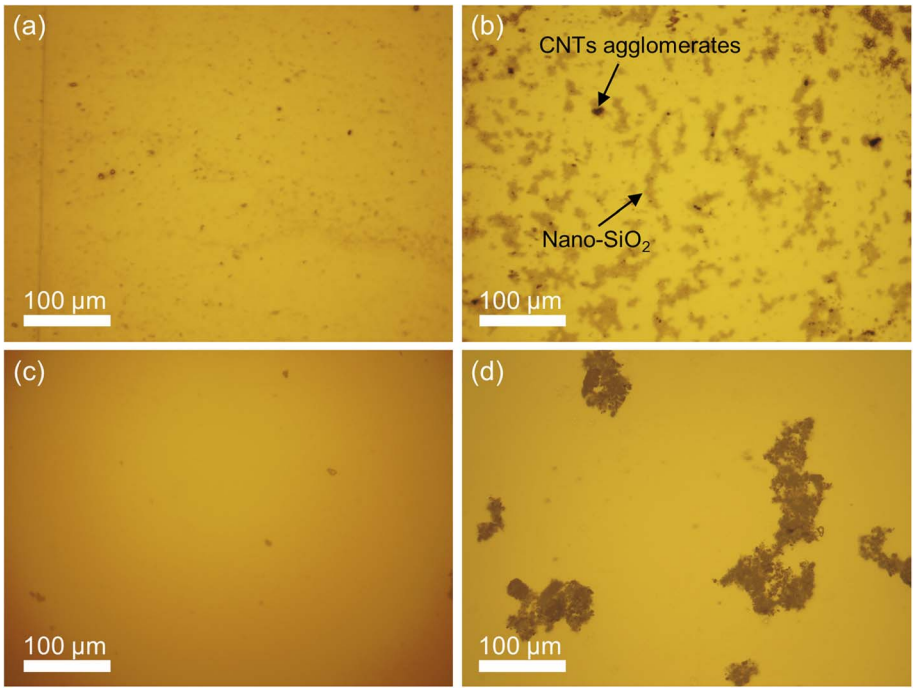

Fig. 8 Optical microscopy images: (a) freshly prepared self-assembled C_1Si_5 suspension; (b) standing for 24 h of C_1Si_5 suspension; (c) freshly prepared CNTs suspension with mass ratio 2 : 1 of CTAB to CNTs; (d) standing for 24 h of CNTs suspension with mass ratio 2 : 1 of CTAB to CNTs.

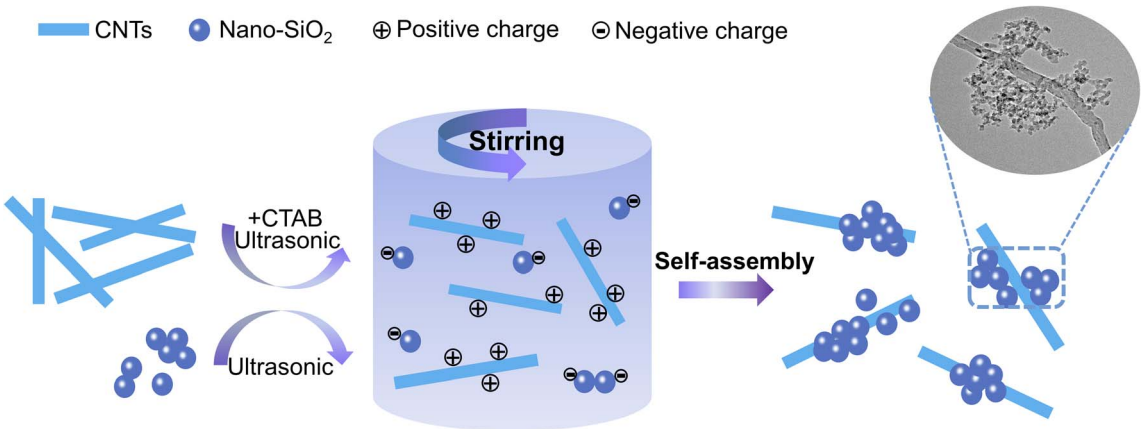

Fig. 9 The schematic illustration of electrostatic self-assembled procedure for CNTs/SiO_2 fillers.

addition of nano-additives, and the toughening effect was more remarkable in samples containing CNTs/SiO_2 fillers. The HC10 (containing 0.10 wt% CNTs and 0.50 wt% nano-SiO_2) showed the highest flexural toughness, and the increase rate reached maximumly about 56%. Even a small fraction of composite fillers, such as HC05 sample, was also sufficient to enhance the toughness of cement mortar matrix by about 40%. The observed phenomenon is closely related to the synergistic effects of CNTs/SiO_2 fillers. The tube-shaped CNTs are advantageous in bridging microcracks, and provide higher resistance to crack propagation at the nanoscale. The nano-SiO_2 particles adsorbed on CNTs surfaces further refine microstructure at the interface between CNTs and cement matrix, thus greatly increasing the energy consumption required for crack growth.

3.4 Morphology and microstructure analysis

In order to further investigate the morphology and microstructure of different specimens, the fracture surfaces of cement composites reinforced by individual CNTs, nano-SiO_2 and CNTs/SiO_2 fillers were observed *via* SEM, as shown in Fig. 12.

For the plain group (Fig. 12(a) and (b)), abundant amount of flake-like CH crystals with different orientations and obvious pores left by free water evaporation were easily observed. The loosely stacked structure is prone to stress concentrations under external loading, which contributes to the brittleness nature of cement matrix.

The typical microstructure of CNTs-reinforced cement mortar is illustrated in Fig. 12(c), indicating that the crack-

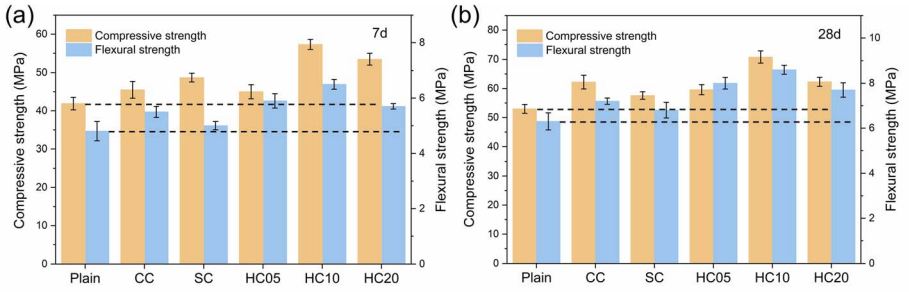

Fig. 10 Mechanical properties of cement mortars at 7 days (a) and 28 days (b).

bridging mechanism of single nanotube is definitely effective in inhibiting crack propagation. It has been found that before fracture or pull-out failure of CNTs there was an intermediate period below a critical width where bridging was effective.[38] These widths ranged from about 0.5 to 3 μm, depending on the concentration, type and aspect ratio of CNTs, and accounted for the aligning, stretching and slipping of CNTs between crack surfaces.[49,50] This mechanism is similar to the role of macro fibers in fiber-reinforced concrete, such as steel fibers and polymer fibers, which promotes strength and toughness increase by delaying crack opening and development.

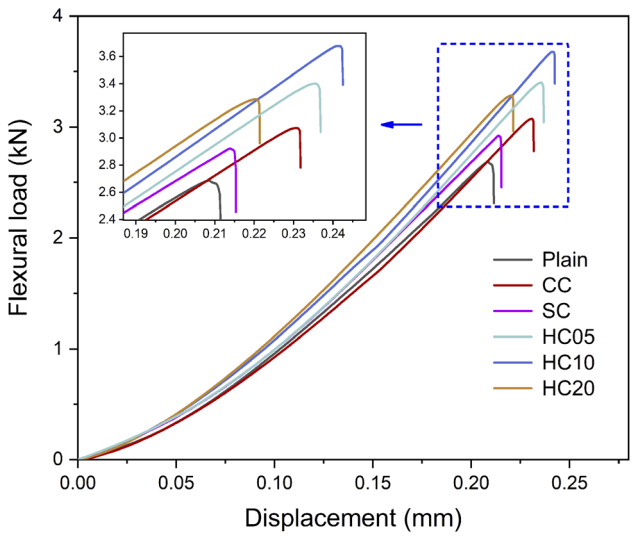

Fig. 11 Flexural load–displacement curves of samples at 28 days.

Table 5 Flexural test result of samples at 28 days and relative flexural toughness

Sample	Maximum load (N)	Displacement (mm)	Area (J)	Relative flexural toughness
Plain	2686	0.208	0.242	1.00
CC	3069	0.231	0.296	1.22
SC	2921	0.213	0.267	1.10
HC05	3402	0.235	0.340	1.40
HC10	3677	0.241	0.377	1.56
HC20	3286	0.220	0.312	1.29

Fig. 12(d) and (e) indicate the fracture features of the HC05 sample, in which many nanoscale pores and cracks can be easily found. Some well-dispersed CNTs were embedded in hydration products, and no CNTs agglomerates were seen during observation. For the HC10 sample containing more CNTs/SiO_2 fillers, as presented in Fig. 12(f) and (g), it can be found that the microstructure was denser and more compact with addition of nano-reinforcers. A number of fine voids instead of big pores distributed among compact hydrated calcium silicate phase (C–S–H) were observed, which mainly resulted from the accelerated hydration reactions by CNTs and pozzolanic activity from nano-SiO_2. In addition, one ends of the well-dispersed CNTs presented pull-out failure (Fig. 12(g)), and the other ends were embedded in hydration products. As the interfacial bonding strength between CNTs and cement matrix is generally lower than the maximum tensile strength of CNTs, the pull-out failure is the dominant failure mechanism.[38] Nevertheless, some CNTs agglomerates and considerable number of micro-flaws occurred in the HC20 group as CNTs/SiO_2 fillers concentration continued to increase (Fig. 12(h)). High concentrations of CNTs/SiO_2 fillers are poorly dispersed of which the suspension features high viscosity, and give rise to lower fluidity as they demand more free water to wet their surfaces. These factors both have negative effects on the mechanical properties of the matrix.

3.5 Hydration characteristics analysis

The hydration characteristics of cement mortar samples reinforced by different nano-additives were determined by TG analysis, as illustrated in Fig. 13. All samples showed similar trend in mass loss variety, and there were four obvious decomposition peaks at corresponding DTG curves. According to other reports, the mass loss below 105 °C is attributed to free water evaporation.[51,52] The mass loss at about 100–200 °C is due to the removal of physically bound water during thermal decomposition of C–S–H gel and ettringite (AFt). The mass loss at about 400–500 °C and 600–700 °C is caused by thermal decomposition of CH and $CaCO_3$ crystals, respectively. Two typical indexes, *i.e.*, the non-evaporable water content and the CH content are commonly employed to estimate the hydration degree of cement, which are calculated based on the following equations.[53]

$$M_{\text{Non-water}} = M_{105^\circ\text{C}} - M_{1000^\circ\text{C}} \quad (1)$$

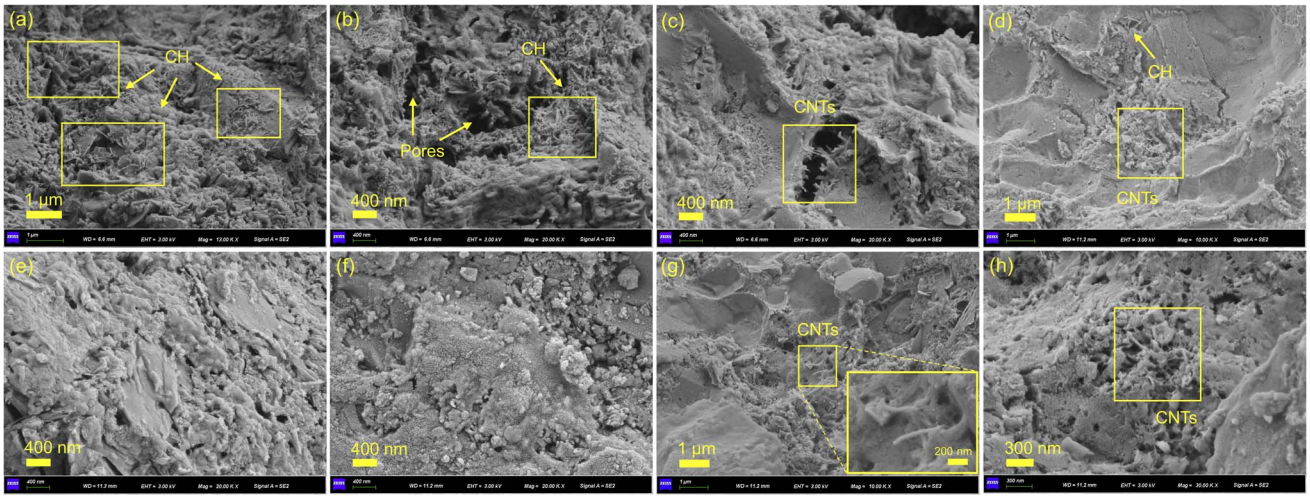

Fig. 12 SEM images of samples at 28 days: (a and b) plain sample; (c) CC; (d and e) HC05; (f and g) HC10; (h) HC20.

$$M_{CH} = \frac{74}{18} \times ML_{CH} + \frac{74}{44} \times ML_{CaCO_3} \quad (2)$$

where $M_{Non\text{-}water}$ is mass percentage of non-evaporable water, $M_{105°C}$ and $M_{1000°C}$ represent the mass percentage of cement composites heated to 105 °C and 1000 °C, respectively. In eqn (2), M_{CH} represents the CH content in percentage, and ML_{CH} is mass loss from CH dehydration. ML_{CaCO_3} represents mass loss caused by $CaCO_3$ decomposition. In addition, 74, 18 and 44 correspond to the molecular weight of CH, H_2O and CO_2, respectively.

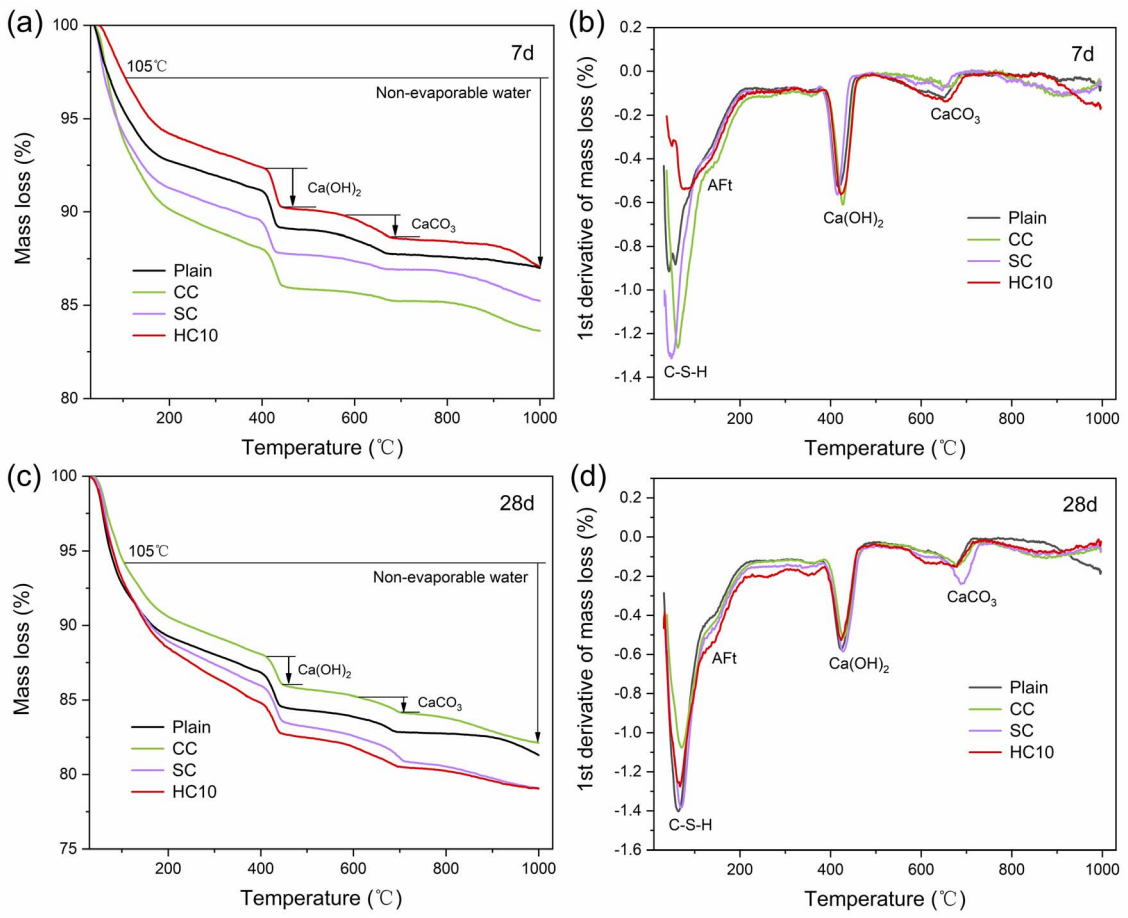

Fig. 13 TG and DTG curves of samples: (a and b) curing for 7 days; (c and d) curing for 28 days.

Table 6 Non-evaporable water and CH content (%) of samples

	7 d		28 d	
Sample	$M_{Non\text{-}water}$	M_{CH}	$M_{Non\text{-}water}$	M_{CH}
Plain	8.26	9.07	1.20	13.98
CC	9.99	9.76	13.72	15.74
SC	8.76	8.80	12.06	12.91
HC10	10.12	10.54	13.79	13.70

As shown in Table 6, the non-evaporable water contents of cement mortar samples reinforced by nano-additives were significantly higher than that of plain sample after curing for 7 and 28 days. These nanoparticles with high specific surface area tend to serve as nucleation sites preferentially for hydration products during the cement hydration, thus imposing positive effects in accelerating hydration process. Noticeably, the HC10 sample displayed the highest non-evaporable water content at all ages, indicating the highest hydration degree brought by CNTs/SiO_2 fillers. Meanwhile, the CH content is a comprehensive reflection of hydration process and pozzolanic reaction by nano-SiO_2 in this paper. It is found that the CH content in HC10 was higher than that of other samples at 7 days. This may be attributed to that the nucleating effects of well-dispersed CNTs/SiO_2 fillers are quite dominant at early ages, and simultaneously a few nano-SiO_2 participate in pozzolanic reaction. After curing for 28 days, the SC and HC10 samples both showed lower CH contents with respect to those of plain and CC samples. It is expected that nano-SiO_2 particles can consume certain amount of CH generated from cement hydration reactions, which are beneficial for refining internal microstructure and enhancing strengths.

Furthermore, the crystalline phases of four kinds of samples during hydration were studied by XRD analysis, and the results are shown in Fig. 14. It deserves to be noted that the C–S–H phase, the main hydration product, featuring low crystallinity like gels, cannot be identified by XRD. Within the detected range by equipment, portlandite (CH), tricalcium silicate (C_3S) and dicalcium silicate (C_2S) are typically selected to analyze

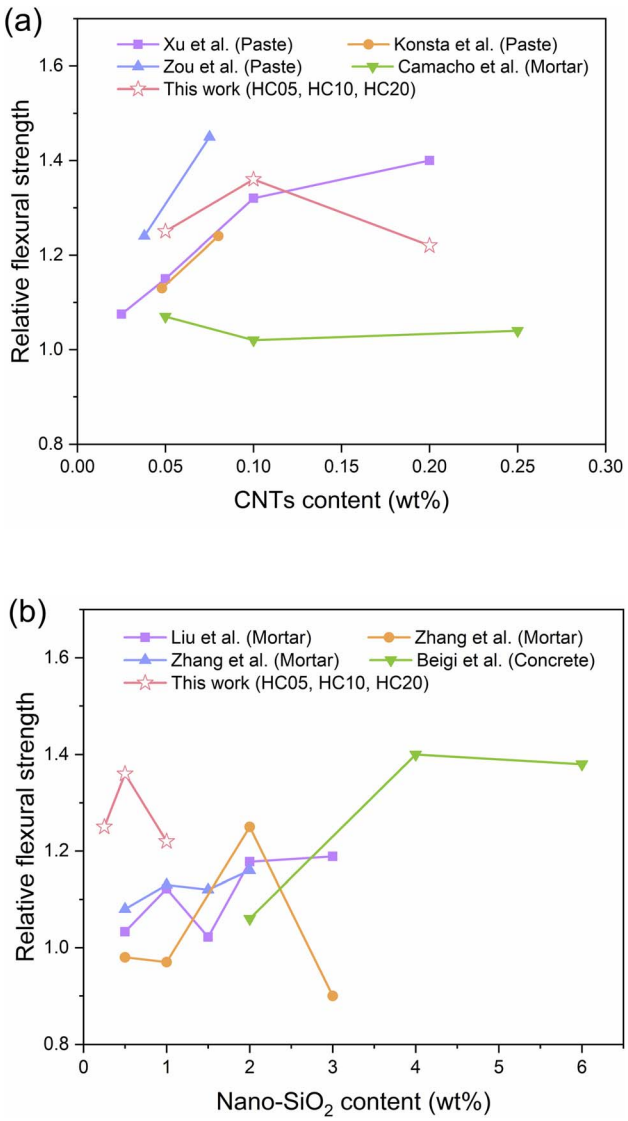

Fig. 15 Comparison results of reinforcement effects on cement materials with addition of CNTs[54–57] (a) and nano-SiO_2 (ref. 23, 24, 40 and 58) (b). Relative flexural strength was calculated with the plain samples as references in different literature.

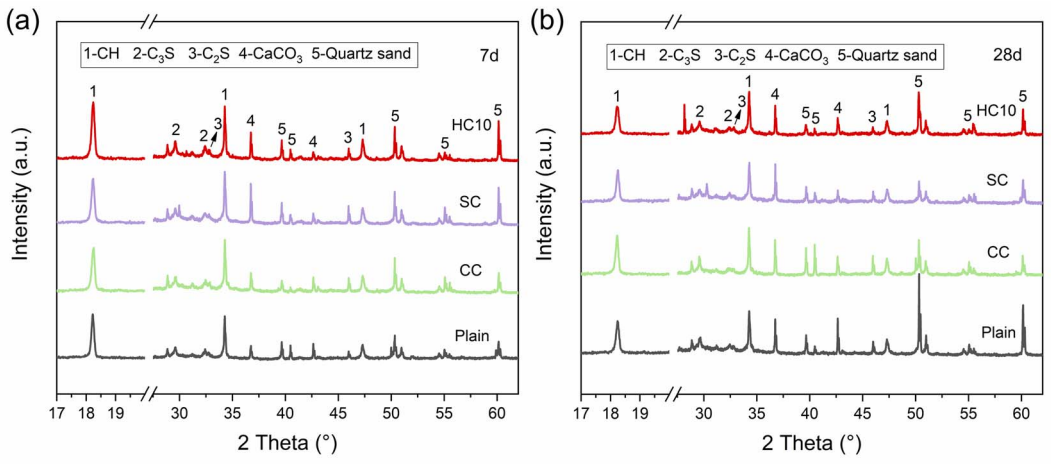

Fig. 14 XRD patterns of samples: (a) curing for 7 days; (b) curing for 28 days.

hydration reaction process, which have been marked at the corresponding diffraction peaks. As the most representative crystalline phase, the peaks of CH were clearly sharper and stronger in the HC10 sample in comparison to others at 7 days, indicating the higher phase content and crystallization. After curing for 28 days, the corresponding peak intensities of CH in SC and HC10 samples were found to be weaker than those of the other samples, especially with respect to the CC sample containing only CNTs, suggesting the effective role of pozzolanic activity by nano-SiO_2. These results are favourably consistent with the TG conclusions discussed above. Therefore, it can be verified that the synergistic effects imposed by CNTs/SiO_2 fillers on cement matrix are definitely effective, including the significant accelerated hydration process by nano-additives and the pozzolanic activity consuming CH by nano-SiO_2.

3.6 Reinforcing mechanisms of CNTs/SiO_2 fillers

The cement composites are more vulnerable to defects when subjected to tension failure, and tend to possess lower flexural strength compared to compressive performance. As shown in Fig. 15, the reinforcing effects on flexural strengths of different nano-additives vary greatly according to previous reports, which are closely related to lots of factors, such as physicochemical features of CNTs, preparation conditions, substrate types, *etc.* Xu *et al.* reported the flexural strengths of cement paste were increased by 30% and 40% with 0.1 wt% and 0.2 wt% CNTs relative to the control.[54] The CNTs were dispersed by an effective surfactant combined with ultrasonication, and the uniform suspension was obtained. In another report, Konsta-Gdoutos *et al.* found that the fracture properties of cementitious matrix greatly improved with incorporation of small amounts of different aspect ratio CNTs.[55] The increase rates on flexural strength with similar CNTs content are slightly lower than that by CNTs/SiO_2 fillers used in this work. More visibly, the lower amounts of nano-SiO_2 employed here still achieve favorable reinforcing effects compared to the dosages proposed by other reports. The maximum increase is performed with addition of 0.5 wt% nano-SiO_2 assembling with 0.1 wt% CNTs, which is only a fourth of dosages used by Liu *et al.*[23] and Zhang *et al.*[24] when they achieve the maximum enhancement results similarly.

The reason which is responsible for above comparison results can be attributed to the synergistic actions of CNTs/SiO_2 fillers, which include the better dispersion stability of CNTs, the nucleating effect of nano-additives and the pozzolanic reaction by nano-SiO_2, thus commonly leading to increased mechanical behavior. The adsorbed nano-SiO_2 particles with certain size on CNTs surfaces alleviate the agglomeration degree of CNTs in aqueous solution, and provide more active sites on CNTs surfaces, as discussed in Section 3.2. With the precondition of stable dispersion, the CNTs/SiO_2 fillers preferentially act as nucleation sites for the growth of hydration products, and then the hydration reactions continue to take place at the growth points at early hydration ages, which has been illustrated in Fig. 16. This greatly promote cement hydration process and improve internal microstructure mainly for C–S–H gels.[35] Meanwhile, the nano-SiO_2 particles with high pozzolanic activity are believed to react with randomly oriented CH crystals, and produce desirable plenty of C–S–H gels, which are greatly beneficial for refining microstructure especially for interfacial area between CNTs and cement matrix. Thus, the hydration products can be bridged by unform CNTs to form a cross-linking structure, resulting in the denser microstructure and higher mechanical properties (Fig. 16(b)). In addition, it should to be noted that the nano-SiO_2 can absorb lots of water to wet their surfaces due to large specific surface area and strong hydrophilicity. Excess amounts of nano-SiO_2 tend to agglomerate again, and increase the viscosity of suspensions of CNTs/SiO_2 fillers. These are detrimental to the fluidity of fresh cement pastes and final strengths (the HC20 sample in this paper), so

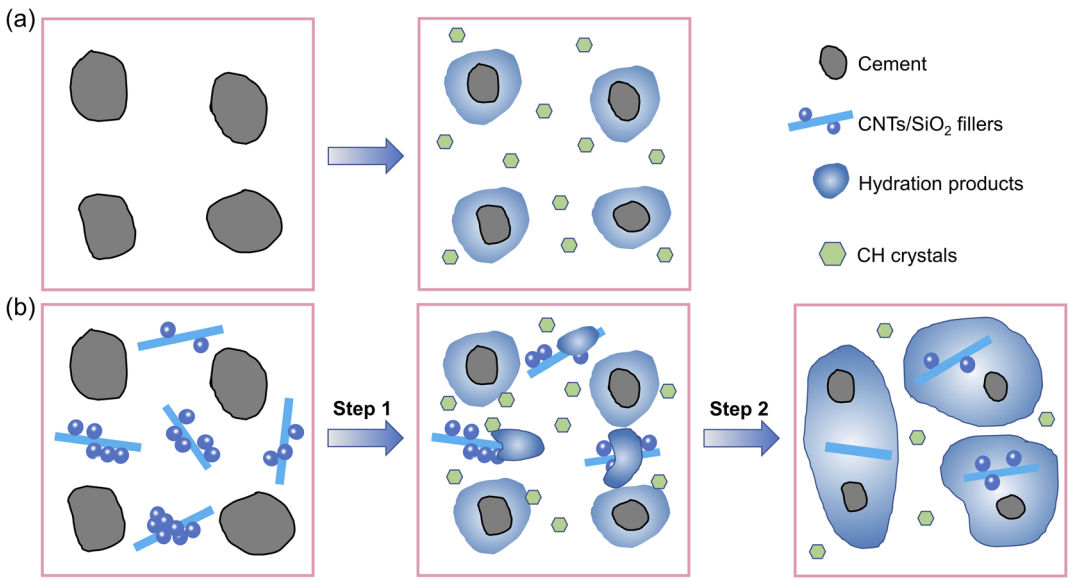

Fig. 16 Schematic illustration of hydration process: (a) traditional cement; (b) the cement reinforced by CNTs/SiO_2 fillers.

determining the appropriate amount of nano-SiO_2 mixing with CNTs is quite important for achieving desirable effects.

4. Conclusions

In summary, this study investigated the hybridization use of CNTs with nano-SiO_2 in cement composites. The CNTs/SiO_2 composite fillers were prepared by electrostatic self-assembly technology. The nano-SiO_2 assembled on positively charged CNTs surface driven by electrostatic interactions, thus forming the approximate "grape string" structure. After examination, it's found that the CNTs inside the fillers tended to unwind due to the mechanical separation and steric hindrance of nano-SiO_2 particles with certain size, and its agglomeration degree in the suspension greatly alleviated over time with enhanced dispersion stability. The optimum assembly ratio of CNTs to nano-SiO_2 was adopted as 1 : 5 by weight.

The synergistic reinforcing effects of the prepared CNTs/SiO_2 composite fillers on cement composites were researched. With the incorporation of CNTs/SiO_2 fillers (0.10 wt% CNTs and 0.50 wt% nano-SiO_2 in the HC10 sample), the flexural and compressive strengths of cement mortars were sharply increased by 33.5% and 36.5% after curing for 28 days compared to the plain sample. Meanwhile, the HC10 sample also showed the highest flexural toughness, and the increase rate reached maximumly about 56.0% with respect to the plain sample. This reinforcing effect by CNTs/SiO_2 fillers was much higher than that of the individual addition of nanomaterials (either CNTs or nano-SiO_2). However, it is worth to note that the continued increasement of the CNTs/SiO_2 fillers content resulted in reduced strengths of cement mortar. The higher fillers concentration could lead to the formation of agglomerates again, which are detrimental to the fluidity and mechanical strengths.

The reinforcing mechanisms of CNTs/SiO_2 fillers were further researched and proposed by means of SEM, TG and XRD analysis. The synergistic effects of CNTs/SiO_2 fillers play an important role in the experiment, which include the improved dispersion stability of CNTs, the nucleating effect of nano-additives and the pozzolanic reaction endowed by nano-SiO_2, thus positively leading to increased mechanical properties. Our work paves an efficient way to take full advantages of nanomaterials in cement composites. In the future, the effects of CNTs assembling with other emerging nanoparticles deserve further investigation to endow cement composites with distinct properties.

Conflicts of interest

There are no conflicts to declare.

Acknowledgements

The authors would like to acknowledge the support for analysis and tests from Shiyanjia Lab (**https://www.shiyanjia.com**).

References

1 G. M. Ren, H. Wu, Q. Fang and J. Z. Liu, *Constr. Build. Mater.*, 2018, **164**, 29–43.
2 Z. Pi, H. Xiao, R. Liu, M. Liu and H. Li, *Composites, Part B*, 2020, **189**, 107904.
3 L. Huang, M. Yuan, B. Wei, D. Yan and Y. Liu, *Constr. Build. Mater.*, 2022, **318**, 125899.
4 T. Si, S. Xie, Z. Ji, C. Ma, Z. Wu, J. Wu and J. Wang, *J. Build. Eng.*, 2022, **45**, 103561.
5 C. Pei, L. Wei, Z. Qin, H. Yu, J.-H. Zhu and F. Xing, *Constr. Build. Mater.*, 2022, **314**, 125506.
6 H. Li, D. Zhao, M. Liebscher, B. Yin, J. Yang, M. Kaliske and V. Mechtcherine, *Cem. Concr. Compos.*, 2022, **128**, 104416.
7 W. Meng and K. H. Khayat, *Composites, Part B*, 2016, **107**, 113–122.
8 D. Zhang, J. Yu, H. Wu, B. Jaworska, B. R. Ellis and V. C. Li, *Composites, Part B*, 2020, **184**, 107741.
9 W. Zhang, X. Zou, F. Wei, H. Wang, G. Zhang, Y. Huang and Y. Zhang, *Composites, Part B*, 2019, **162**, 500–507.
10 J. Feng, X. Gao, J. Li, H. Dong, W. Yao, X. Wang and W. Sun, *Composites, Part B*, 2019, **163**, 487–496.
11 H. Yang, H. Cui, W. Tang, Z. Li, N. Han and F. Xing, *Composites, Part A*, 2017, **102**, 273–296.
12 F. Basquiroto de Souza, X. Yao, J. Lin, Z. Naseem, Z. Q. Tang, Y. Hu, W. Gao, K. Sagoe-Crentsil and W. Duan, *Constr. Build. Mater.*, 2022, **324**, 126636.
13 M. Ramezani, Y. H. Kim and Z. Sun, *Cem. Concr. Compos.*, 2019, **104**, 103347.
14 L. Silvestro, P. Jean and P. Gleize, *Constr. Build. Mater.*, 2020, **264**, 120237.
15 B. Şimşek, *J. Build. Eng.*, 2020, **32**, 101792.
16 Y. Suo, R. Guo, H. Xia, Y. Yang, B. Zhou and Z. Zhao, *J. Build. Eng.*, 2022, **53**, 104502.
17 J. Wang, S. Dong, S. D. Pang, C. Zhou and B. Han, *Cem. Concr. Compos.*, 2022, **128**, 104453.
18 A. M. Onaizi, G. F. Huseien, N. H. A. S. Lim, M. Amran and M. Samadi, *Constr. Build. Mater.*, 2021, **306**, 124850.
19 S. C. Paul, A. S. van Rooyen, G. P. A. G. van Zijl and L. F. Petrik, *Constr. Build. Mater.*, 2018, **189**, 1019–1034.
20 P. Sikora, M. Abd Elrahman, S.-Y. Chung, K. Cendrowski, E. Mijowska and D. Stephan, *Cem. Concr. Compos.*, 2019, **95**, 193–204.
21 B. Han, Z. Li, L. Zhang, S. Zeng, X. Yu, B. Han and J. Ou, *Constr. Build. Mater.*, 2017, **148**, 104–112.
22 H. Li, M. Zhang and J. Ou, *Wear*, 2006, **260**, 1262–1266.
23 J. Liu, Q. Li and S. Xu, *Constr. Build. Mater.*, 2015, **101**, 892–901.
24 A. Zhang, W. Yang, Y. Ge, Y. Du and P. Liu, *J. Build. Eng.*, 2021, **34**, 101936.
25 J. Xu, S. Ashraf, S. Khan, X. Chen, A. Akbar and F. Farooq, *J. Build. Eng.*, 2021, **42**, 102816.
26 F. Li, L. Liu, Z. Yang and S. Li, *Ceram. Int.*, 2021, **47**, 907–922.
27 P. Stynoski, P. Mondal and C. Marsh, *Cem. Concr. Compos.*, 2015, **55**, 232–240.

28 D. Lu, X. Shi and J. Zhong, *Cem. Concr. Compos.*, 2022, **126**, 104366.
29 Y. Wang, Y. Alrefaei and J. Dai, *Constr. Build. Mater.*, 2021, **306**, 124880.
30 S. J. Chen, W. Wang, K. Sagoe-Crentsil, F. Collins, X. L. Zhao, M. Majumder and W. H. Duan, *RSC Adv.*, 2016, **6**, 5745–5753.
31 J. C. Grunlan, L. Liu and O. Regev, *J. Colloid Interface Sci.*, 2008, **317**, 346–349.
32 Y. Gao, H. Jing, M. Du and W. Chen, *Nanomaterials*, 2018, **8**, 858.
33 A. M. Sabziparvar, E. Hosseini, V. Chiniforush and A. H. Korayem, *Constr. Build. Mater.*, 2019, **199**, 269–278.
34 B. S. Sindu and S. Sasmal, *Constr. Build. Mater.*, 2020, **253**, 119190.
35 Y. Li, H. Li, Z. Wang and C. Jin, *Cem. Concr. Res.*, 2020, **128**, 105955.
36 L. Lavagna, R. Nisticò, S. Musso and M. Pavese, *Mater. Today Chem.*, 2021, **20**, 100477.
37 A. Akbar, V. K. R. Kodur and K. M. Liew, *Cem. Concr. Compos.*, 2021, **121**, 104069.
38 H. Ahmed, J. A. Bogas, M. Guedes and M. F. C. Pereira, *Mag. Concr. Res.*, 2019, **71**, 408–423.
39 Y. Qing, Z. Zenan, K. Deyu and C. Rongshen, *Constr. Build. Mater.*, 2007, **21**, 539–545.
40 L. Zhang, N. Ma, Y. Wang, B. Han, X. Cui, X. Yu and J. Ou, *J. Compos. Mater.*, 2016, **50**, 4135–4146.
41 R. Liu, H. Xiao, J. Geng, J. Du and M. Liu, *Constr. Build. Mater.*, 2020, **244**, 118297.
42 L. Wu, Z. Lu, C. Zhuang, Y. Chen and R. Hu, *Materials*, 2019, **12**, 3773.
43 M. Lu, H. Xiao, M. Liu, X. Li, H. Li and L. Sun, *Cem. Concr. Compos.*, 2018, **91**, 21–28.
44 L. Vaisman, G. Marom and H. D. Wagner, *Adv. Funct. Mater.*, 2006, **16**, 357–363.
45 Y. Liu, W. Jiang, S. Li and F. Li, *Appl. Surf. Sci.*, 2009, **255**, 7999–8002.
46 N. Wang, S. Pandit, L. Ye, M. Edwards, V. R. S. S. Mokkapati, M. Murugesan, V. Kuzmenko, C. Zhao, F. Westerlund, I. Mijakovic and J. Liu, *Carbon*, 2017, **111**, 402–410.
47 R. Alfonsetti, G. De Simone, L. Lozzi, M. Passacantando, P. Picozzi and S. Santucci, *Surf. Interface Anal.*, 1994, **22**, 89–92.
48 F. Wang, S. Lin, X. Lu, R. Hong and H. Liu, *Electrochim. Acta*, 2022, **404**, 139708.
49 L. Zhao, X. Guo, C. Ge, Q. Li, L. Guo, X. Shu and J. Liu, *Composites, Part B*, 2017, **113**, 308–316.
50 R. Nadiv, M. Shtein, M. Refaeli, A. Peled and O. Regev, *Cem. Concr. Compos.*, 2016, **71**, 166–174.
51 X. Cui, B. Han, Q. Zheng, X. Yu, S. Dong, L. Zhang and J. Ou, *Composites, Part A*, 2017, **103**, 131–147.
52 M. Liu, J. Lei, L. Guo, X. Du and J. Li, *Thermochim. Acta*, 2015, **613**, 54–60.
53 A. Peschard, A. Govin, P. Grosseau, B. Guilhot and R. Guyonnet, *Cem. Concr. Res.*, 2004, **34**, 2153–2158.
54 S. Xu, J. Liu and Q. Li, *Constr. Build. Mater.*, 2015, **76**, 16–23.
55 M. S. Konsta-Gdoutos, Z. S. Metaxa and S. P. Shah, *Cem. Concr. Res.*, 2010, **40**, 1052–1059.
56 B. Zou, S. J. Chen, A. H. Korayem, F. Collins, C. M. Wang and W. H. Duan, *Carbon*, 2015, **85**, 212–220.
57 M. del C. Camacho, O. Galao, F. J. Baeza, E. Zornoza and P. Garcés, *Materials*, 2014, **7**, 1640–1651.
58 M. H. Beigi, J. Berenjian, O. L. Omran, A. S. Nik and I. M. Nikbin, *Mater. Des.*, 2013, **50**, 1019–1029.